Viewing Dynamic Assembly of Molecular Complexes by Multi-Wavelength Single-Molecule Fluorescence

Larry J. Friedman, Johnson Chung, and Jeff Gelles
Department of Biochemistry, Brandeis University, Waltham, Massachusetts

ABSTRACT Complexes of macromolecules that transiently self-assemble, perform a particular function, and then dissociate are a recurring theme in biology. Such systems often have a large number of possible assembly/disassembly intermediates and complex, highly branched reaction pathways. Measuring the single-step kinetic parameters in these reactions would help to identify the functionally significant pathways. We have therefore constructed a novel single-molecule fluorescence microscope capable of efficiently detecting the colocalization of multiple components in a macromolecular complex when each component is labeled using a different color fluorescent dye. In this through-objective excitation, total internal reflection instrument, the dichroic mirror conventionally used to spectrally segregate the excitation and emission pathways was replaced with small broadband mirrors. This design spatially segregates the excitation and emission pathways and thereby permits efficient collection of the spectral range of emitted fluorescence when three or more dyes are used. In a test experiment with surface-immobilized single-stranded DNA molecules, we directly monitored the time course of a hybridization reaction with three different oligonucleotides, each labeled with a different color dye. The experiment reveals which of the possible reaction intermediates were traversed by each immobilized molecule, measures the hybridization rate constants for each oligonucleotide, and characterizes kinetic interdependences of the reaction steps.

INTRODUCTION

A wide variety of biological processes, including signal transduction, transcription regulation, DNA replication, and RNA splicing, are performed by complexes of multiple noncovalently associated macromolecules. Often, such complexes assemble transiently to initiate a process and then dissociate upon completion of their function. There may be multiple changes in the constituents and configuration of the complex as the reaction progresses. In the regulation of transcription initiation, for example, most genes are regulated by multiple transcription factor proteins that bind to target DNA sites in the vicinity of the promoter and collectively influence whether the gene is expressed or remains silent. Since each site can be occupied by a protein or vacant, there are many (typically tens or even hundreds of) distinct arrangements or states of the protein-DNA complex. Understanding the dynamic functioning of such a system at the molecular level requires knowing i), the reaction pathway and kinetics by which the complex progresses through its different states, ii), the extent to which the gene is activated in each state, and iii), the ways these properties are altered in response to environmental stimuli. Such information is not readily attainable in conventional biochemical experiments which study the average properties of populations of complexes, because such populations are in general mixtures of many different states.

In principle, the advent of single molecule fluorescence microscopy provides an attractive way to circumvent these difficulties. Individual protein or nucleic acid components of the complex could each be labeled by a different color fluorescent dye. The progress of the reaction could then be monitored by measuring the time course of the emission intensities of the various colors, which would then reflect the identities and number of the different macromolecular species present in the complex at any time.

Single-molecule fluorescence microscopy imaging of two colors of dyes has been used to study biochemical mechanisms in a variety of systems. For example, colocalized imaging of both a myosin motor enzyme and a dye-labeled ATP analog allowed direct detection of substrate binding and product release in single enzyme molecules (1). Excitation and detection of two dyes were employed in fluorescence resonance energy transfer (FRET) experiments that identified rate-limiting steps in the abortive initiations preceding promoter escape by RNA polymerase (2). Recording emissions from two dyes was also central to the FRET experiments that determined the mechanism of Rep helicase (3), characterized multiple states in ribosomal tRNA selection (4), and monitored folding of proteins and RNA (5,6). Single-molecule three-color FRET has been implemented (with one donor excitation laser and three detection channels) to probe correlated motions within a single Holliday junction (7).

Many biological complexes of interest have more than two macromolecular components. Mechanistic analysis of multicomponent systems by colocalization of dye-labeled macromolecules would be facilitated by the ability to simultaneously excite and detect the presence of more than two dyes. However, single-molecule fluorescence microscopes must efficiently collect emitted photons because of the limited number

Submitted February 24, 2006, and accepted for publication April 14, 2006.

Address reprint requests to Larry J. Friedman, E-mail: larryfj@brandeis.edu; or Jeff Gelles, E-mail: gelles@brandeis.edu.

0006-3495/06/08/1023/09 $2.00

doi: 10.1529/biophysj.106.084004

of photons produced from each dye before photobleaching. Unfortunately, with existing single molecule fluorescence microscope designs, the incorporation of optics for selective excitation and detection of more than two dyes can cause such a significant reduction in photon collection efficiency that single-molecule detection becomes impracticable.

We here report a new single-molecule fluorescence microscope design capable of simultaneously exciting and efficiently collecting emission from three or more spectrally separated dye molecules. In a test application of this design, we use the microscope to detect the binding of three dye-labeled oligonucloetides complementary to different segments of single immobilized DNA molecules. The resulting data yield measurements of single reaction step kinetics and reveal the preferred reaction pathways in this complex multi-strand hybridization reaction.

METHODS AND MATERIALS

Oligonucleotides

Dye- or biotin-tagged DNA oligonucleotides were purchased from IDT (Coralville, IA). The Cy5, Cy3, and Alexa 488-tagged probe molecules were 5′−GTGTGTGGTCTGTGGTGTCT/Cy5/−3′, 5′−GTGTCCCTCTCGAT/Cy3/−3′ and 5′−/Alexa488/AGGGTTTTCCCAGTCACGAC-3′. The sequence for the surface-tethered biotin-ssDNA was 5′−/Bio/CCAAAGACACCACAGACCACACACAAGAATCGAGAGGGACACCAACGTCGTGACTGGGAAAACCCT−3′, where the sequences complementary to the Cy5, Cy3, and Alexa 488 oligonucleotides are shown with single-underline, dotted underline, and bold type, respectively.

Sample preparation

Flow chambers for microscopy were prepared with two glass or one glass and one fused silica (Bond Optics; Lebanon, NH) coverslips that were cleaned (3) and then derivatized with an aminosilane reagent (Vectabond, Vector Laboratories; Burlingame, CA) according to the manufacturer's instructions except that the acetone presoak was eliminated to reduce background surface fluorescence. The coverslip surfaces were then derivatized with a mixture of succinimidyl (NHS) polyethylene glycol (PEG), and NHS-PEG-biotin (Nektar; Huntsville, AL) as described (3), with the following modifications: NHS-PEG and NHS-PEG-biotin were stored under dry nitrogen gas at −20°C. Into a flow cell lane delimited by lines of silicone vacuum grease sandwiched between the two coverslips (typical volume 20 μl), we introduced freshly prepared 20% (w/w) NHS-PEG, 0.20% (w/w) NHS-PEG-biotin, 0.1 M $NaHCO_3$, pH 8.3. The cell was incubated >3 h, then washed with 5 × 100 μl water and then with 2 × 100 μl 0.1 mg/ml bovine serum albumin (126615; Calbiochem; San Diego, CA), 50 mM Tris acetate pH 8.0, 100 mM potassium acetate, 8 mM magnesium acetate, and 27 mM ammonium acetate. All subsequent DNA additions and washes used this solution. Typically, biotin-ssDNA was introduced at 160 pM and incubated 30 min. To initiate the hybridization reaction, a solution containing the three dye-labeled oligonucleotides supplemented with an O_2 scavenging system (8) was introduced into the cell.

Microscope

The imaging system was constructed as an optical table microscope using commercially available hardware and optics. The sample slides were mounted atop a precision three-axis piezoelectric translation stage (Mad City Labs; Madison, WI) used for z focus and for x-y calibration of the magnification. The piezoelectric stage itself was mounted on a manual translation stage used for coarse positioning. The 100× 1.45 NA Plan-Fluar objective (Zeiss; Thornwood, NY) was positioned in inverted orientation in a fixed mount with its internal spring held in maximum compression by a machined collar. Two 2.0 × 2.8-mm ellipsoidal mirrors (G54-092, Edmund Optics; Barrington, NJ) used to direct the excitation beam were positioned ~1 mm from the bottom of the objective lens. The laser beam in this region is rapidly converging, and this small lens-mirror separation serves to minimize the intrusion of the mirrors into the imaging path. Each mirror was cemented onto the end of a threaded rod, which was screwed into a miniature post/post holder (Newport, Irvine, CA) positioned using a miniature three-axis stage. Fixed positioning of the objective and compression of the spring were required to achieve and maintain the small mirror in alignment with and in close proximity to the final lens element of the objective. Where necessary, other optics were rail mounted to allow repositioning to accommodate the different refractive indices of glass and fused silica coverslips. The same immersion oil (refractive index 1.516; Olympus; Melville, NY) was used with both coverslip materials.

Microscope operation and image acquisition were controlled by custom software (9) implemented with LabView (National Instruments; Austin, TX). This software also operated the laser shutters (Uniblitz, Vincent Associates; Rochester, NY) and the electron multiplying charge coupled device (EMCCD) camera (iXon 87, Andor Technology; South Windsor, CT, or Cascade 512b, Photometrics; Tucson, AZ). Uncompressed digital images were streamed continuously to disk; each frame was identified with respect to both the excitation wavelength and acquisition time to facilitate subsequent reconstruction and analysis of the image sequence. Offline image analysis was performed with custom software implemented with MATLAB (The MathWorks; Natick, MA). Image alignment between the two fields of the dual view apparatus was performed using a function that accommodates small fixed differences in the relative magnifications and rotational orientations of the two fields. Intensity calibration of the camera is described in the Supplementary Material.

RESULTS

Microscope design: rationale

For the observation of single fluorescing molecules, it is desirable to reduce background fluorescence by minimizing the volume of solution in which fluorescence is excited. One way to reduce the excitation volume is through the use of a total internal reflection (TIR) microscope (1,10), in which excitation is confined to a ~100-nm-thick solution layer above a glass surface. In a common single-molecule TIR fluorescence microscope design (11), a narrow beam from the excitation laser is introduced at the extreme edge of the exit pupil of a high numerical aperture (NA) objective lens (Fig. 1 *a*). This causes the excitation to strike the glass-solution interface obliquely, producing TIR at that interface. A long-pass dichroic mirror is used to direct the excitation into the objective and to selectively exclude both reflected and scattered excitation light from the optics that image the longer wavelength fluorescence emission.

Dichroic mirrors with multiple reflection bands can be employed to adapt this design to experiments with multiple dyes that are excited and emit at different wavelengths. However, such multi-band filters have reduced pass-band transmission and broadened reflection bands, leading to greatly reduced emitted photon collection efficiencies, particularly when more than two dyes are used. To avoid such losses, we built a multi-wavelength single-molecule fluorescence microscope that

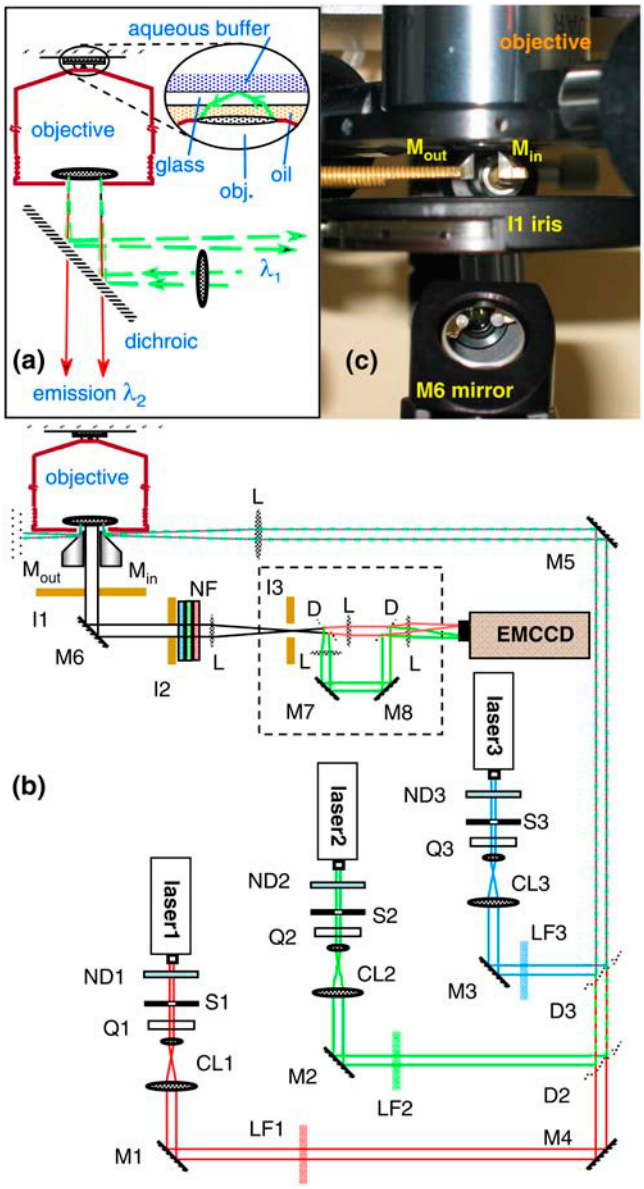

FIGURE 1 Optical layouts for TIR fluorescence microscopes. (*a*) Conventional through-objective TIR. The incoming short-wavelength (λ_1) excitation beam is reflected by a dichroic mirror, passes through the objective lens, and is totally internally reflected at the glass-aqueous interface (*inset*). The longer-wavelength (λ_2) fluorescence emission is transmitted through the dichroic. (*b*) Schematic layout (not to scale) of the multi-wavelength single-molecule TIR fluorescence microscope. The design incorporates two small broadband mirrors (M) for directing multi-wavelength laser excitation into the objective (M_{in}) and deflecting the reflected laser beam that exits the objective away from the image path (M_{out}). Fluorescence emission is transmitted through the gap between the mirrors. ND, neutral density filter; S, shutter; Q, quarter-wave plate; CL, collimating lens pair; LF, laser filter; D, dichroic; L, lens; I, iris; and NF, long-pass (HQ505LP, Chroma Technology; Rockingham, VT) and 532/633 nm dual notch filter (Barr Associates; Westford, MA) filters; EMCCD, electron multiplying charge-coupled device camera. The dashed box encloses the dual view optics. (*c*) Photograph showing the physical arrangement of the objective and optics M_{in}, M_{out}, I1, and M6 in the multi-wavelength microscope.

eliminates the oblique dichroic mirror and instead allocates spatially separate portions of the objective lens aperture to pass the excitation and emission beams. This design permits simultaneous excitation at multiple wavelengths, collects fluorescence emission efficiently, and minimizes background caused by autofluorescence in the microscope optics.

Microscope design: implementation

To excite the sample at multiple wavelengths simultaneously, three laser beams of different wavelengths are combined using dichroic mirrors and focused onto the back focal plane of the objective (Fig. 1 *b*). Computer-controlled mechanical shutters allow use of individual or any combination of excitation wavelengths. A small mirror positioned just beneath the objective directs the combined input beam to just inside the edge of the objective back aperture to achieve TIR excitation at the coverslip-aqueous interface. A second mirror at the opposite edge of the back aperture directs the reflected laser excitation into a beam dump. Off-axis secondary reflections are removed by iris diaphragm I2. Notch filters with ~6 optical density at each excitation wavelength remove residual laser scatter from the emission. Dual view optics (3,12) are used to form on a single camera two separated images of emission less than and greater than 635 nm.

Efficient transmission of emitted fluorescence through the objective is essential to good performance of a single-molecule fluorescence microscope. In principle, the small mirrors used to direct the excitation lasers could significantly obstruct the objective aperture, reducing transmission. In our implementation this obstruction is insignificant, with the mirrors

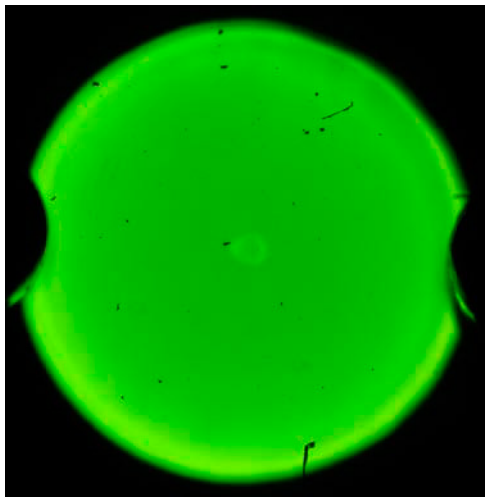

FIGURE 2 Transmission of emitted fluorescence through the objective back aperture. Fluorescence from a flow chamber with surface-adsorbed fluorescent beads (F8786, Molecular Probes; Eugene, OR) excited at 532 nm is observed looking at the objective back aperture through a Bertrand lens positioned after M6 (see Fig. 1 *b*). The green region is the portion of the aperture through which emitted fluorescence is transmitted. The small areas blocked by the input and output mirrors are seen as semicircular outlines at left and right.

blocking only 4% of the active aperture (Fig. 2). In contrast, a conventional microscope design with a dichroic mirror (Fig. 1 *a*) utilizes the full objective aperture but suffers significant loss of emission due to reduced spectral bandwidth. The reduced bandwidth is a consequence of the requirement that the dichroic must reflect light of the wavelengths used for excitation. For example, using the transmission spectrum for a commercially available dichroic mirror with three reflection bands appropriate for our laser wavelengths, we calculate that only 53% of the Alexa488 and 54% of the Cy3 fluorescence emission would pass through this optic into the imaging path.

In addition to eliminating the need for wavelength-selective optics common to the excitation and emission pathways, the small mirrors used to introduce the multi-wavelength excitation beam serve to significantly reduce background autofluorescence. In any microscope design in which the excitation light passes through the objective (''epi-illumination''), it excites some background fluorescence in the glass lens elements and cements within the objective itself. When the beam exit mirror (M_{out} in Fig. 1 *b*) is removed, a prominent autofluorescence spot is visible at the position in the objective back aperture where the beam exits (Fig. 3 *a*). This background is blocked from entering the imaging pathway when the mirror is replaced, leaving only a faint autofluorescence line between the two mirrors (Fig. 3 *b*). (The line is the side view of the beam as it traverses the objective.) Measurements under single dye molecule imaging conditions indicate that the small mirrors reduce the intensity of background from autofluorescence by ~1.5-fold. An even larger amount of autofluorescence is emitted off the optical axis and is blocked by iris diaphragms I1 and I2.

Single dye molecule imaging

To make sustained observations of single fluorescent dye molecules in an aqueous environment, we observed samples in which single-stranded DNA molecules immobilized on a coverslip surface at low density were hybridized to one or more dye-labeled oligonucleotides (Fig. 4).

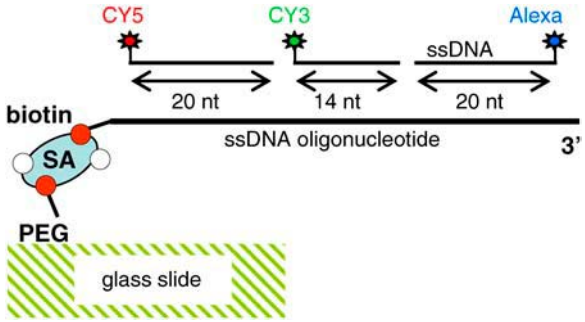

FIGURE 4 Preparation of surface-immobilized DNAs labeled with individual dye molecules that fluoresce at one or more wavelengths. Single-stranded DNA molecules were tethered to a PEG-coated slide surface through biotin-streptavidin (SA) linkages. DNA quantity was limited to produce a surface density $\ll 1$ molecule per diffraction-limited spot. One or more dye-labeled oligonucleotides introduced into the flow cell can then hybridize with this surface-tethered ssDNA.

Single dye molecules image as diffraction-limited spots, and we examined these spots to verify that the mirror intrusion on the imaging path did not degrade the microscope point spread function or photon flux. Spots were approximately Gaussian with a full width at half-maximum (FWHM = $2.35\sigma_x = 288$ and $2.35\sigma_y = 313$ nm in Fig. 5) in agreement with prior measurements from single-molecule microscopes (13) and comparable to that expected for the diffraction limit ($0.61\ \lambda/\mathrm{NA} = 266$ nm for a $\lambda = 580$ nm emission wavelength and an NA = 1.33 effective NA that is limited by the refractive index of the buffer surrounding the fluorophores). With a low autofluorescence-fused silica coverslip, the spot FWHM increased to ~335 nm due to aberrations resulting from the lower refractive index of the coverslip.

The number of photons emitted by the dye molecule before photobleaching and the efficiency with which the microscope detects these photons are usually the principal limiting factors in the application of single-molecule fluorescence to the study of biochemical processes in vitro. To verify that the microscope efficiently collects and registers fluorescence emission, we calibrated the camera output (see Supplementary Material) and then measured the number of

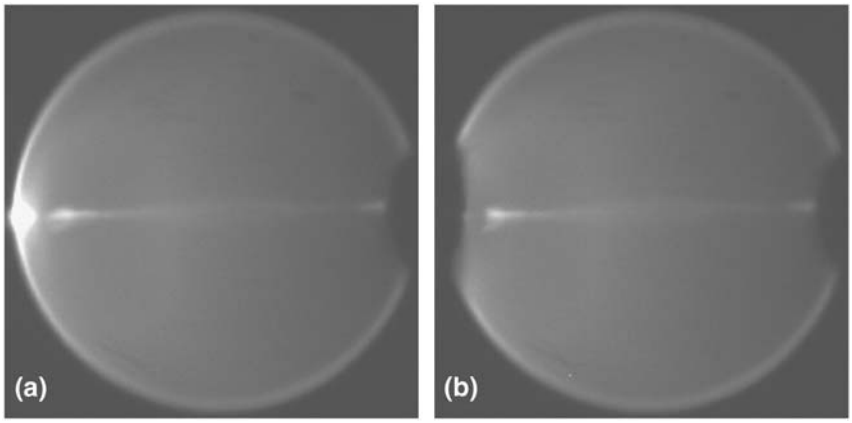

FIGURE 3 Removal of objective lens autofluorescence by the laser coupling mirrors. Images show the objective back focal plane as imaged with the EMCCD camera without (*a*) and with (*b*) the output mirror M_{out} (see Fig. 1 *b*) in place. A sample on a glass coverslip of aqueous buffer without any fluorophore was excited at 532 nm, 0.7 mW incident power. Filters attenuating the 532-nm excitation wavelength by 10^{12}-fold were present in the imaging path. Alterations of the attenuation factor caused a far less than proportional change in the observed spot intensity (data not shown), indicating that the spot is autofluorescence rather than scattered or reflected excitation light.

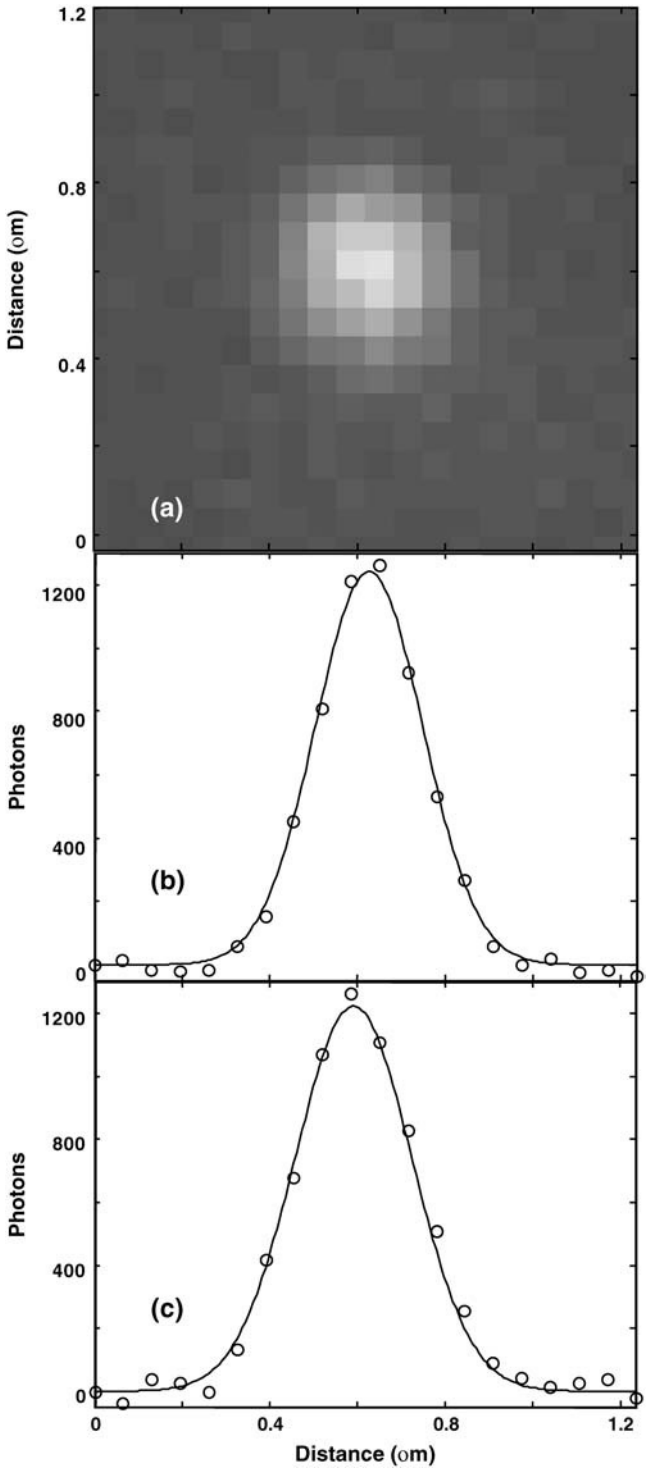

FIGURE 5 Image of a single Cy3-labeled DNA molecule. (*a*) Image acquired over 1.5 s. The integrated spot is comprised of ~30,000 photons. (*b* and *c*) The central *x* row (*b*) and *y* column (*c*) of pixel intensities (*points*) together with the corresponding values (*lines*) from the fit of the image to the two-dimensional Gaussian $\exp[-(x-x_o)^2/(2\sigma_x^2) - (y-y_o)^2/(2\sigma_y^2)]$.

photons emitted before photobleaching from a population of DNA molecules containing single Cy3 dyes. We record $>2 \times 10^6$ photons from 65% of the Cy3-DNA constructs and $>7 \times 10^6$ from 15% (Fig. 6), yields which are comparable to those obtained with a conventional TIR microscope (13). The somewhat nonexponential character of the distribution in Fig. 6 may arise from nonuniform excitation across the microscope field combined with the fact that single dye photon yields from Cy3-DNA vary with excitation intensity (data not shown). Taken together, the photobleaching and spot width measurements confirm that the mirror intrusions into the image path do not appreciably degrade the point spread function or diminish the photon collection efficiency.

High signal/noise ratios (S/N) were obtained when the microscope was used to record the fluorescence from single dye-labeled DNA molecules, even at excitation powers sufficiently low to permit acquiring hundreds or thousands of time points before dye photobleaching. In an example record obtained with a fused silica coverslip (Fig. 7 *a*), the dye S/N is 14.8, allowing determination of the presence or absence of the dye in each time point with high certainty ($P < 10^{-6}$). Records obtained with a glass coverslip (e.g., Fig. 7 *b*) have higher noise due to the larger coverslip autofluorescence. Glass autofluorescence is even more severe in the >635-nm images of the dual view optics (data not shown). The large reduction of noise upon photobleaching in Fig. 7 *a* demonstrates that the variability in the single dye signal with a fused silica coverslip is dominated by photon shot noise. In this instance, only an insignificant fraction (~5%) of the dye signal standard deviation is contributed by noise from the background fluorescence. Thus, the background signal is already sufficiently low that improvements to microscope design that further reduce background would not significantly increase the quality of the records. The selection of glass or fused silica depends on whether the smaller point spread function obtained with the former is of more value in

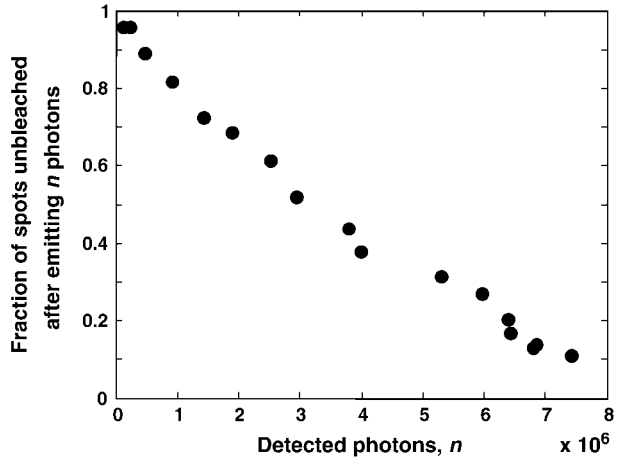

FIGURE 6 Photobleaching statistics for 137 Cy3-DNA molecules. Images were obtained with 0.7-mW incident 532-nm excitation.

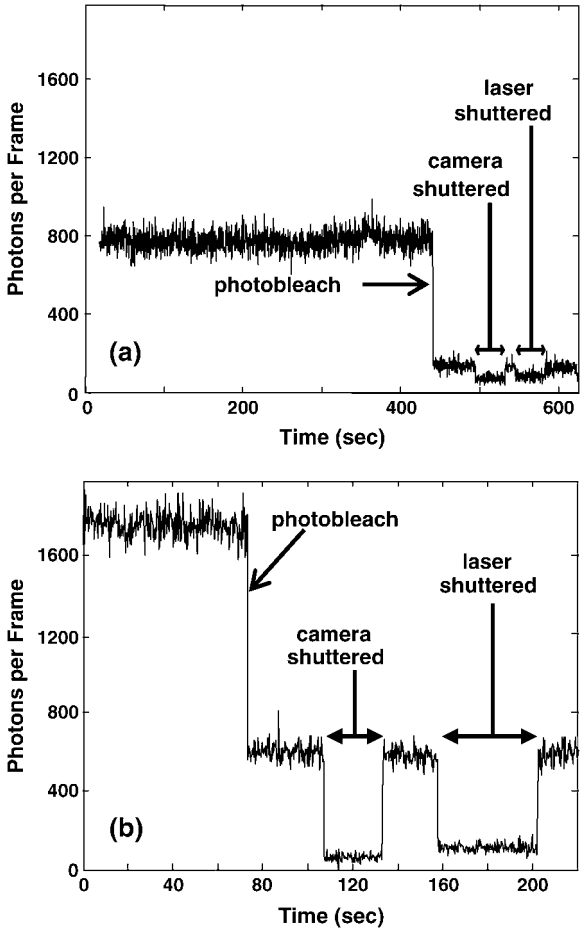

FIGURE 7 Time records of fluorescence from single Cy3-DNA molecules immobilized on fused silica (*a*) or glass (*b*) coverslips. Emission at wavelengths <635 nm from a 0.8-μm^2 (*a*) or 0.4-μm^2 (*b*) area was recorded with 0.2-s time resolution using 0.7-mW 532-nm excitation. After dye photobleaching (*arrows*), the camera and excitation laser were sequentially shuttered to record the relative amounts of background noise caused by camera noise, stray light, and autofluorescence.

a particular application than the reduced noise obtained with the latter.

Multi-wavelength imaging and single-molecule kinetics

The microscope affords an efficient design for observing single-molecule fluorescence from multiple colors of dyes simultaneously. A coverslip surface sparsely decorated with DNA molecules containing the fluorescent dyes Alexa 488, Cy3, and Cy5 (Fig. 4) shows readily visible spots from each kind of dye (Fig. 8). Photobleaching occurred in single steps (not shown), confirming that the spots are single dye molecules. Which dyes are present in each DNA molecule can be readily determined by shuttering the excitation lasers and/or by using the emission wavelength selection afforded by the dual-view optics (Fig. 8 *f*). Even when all three lasers are on simultaneously (Fig. 8, *d* and *e*), the background fluorescence is sufficiently low that single molecules are imaged with high S/N ratios.

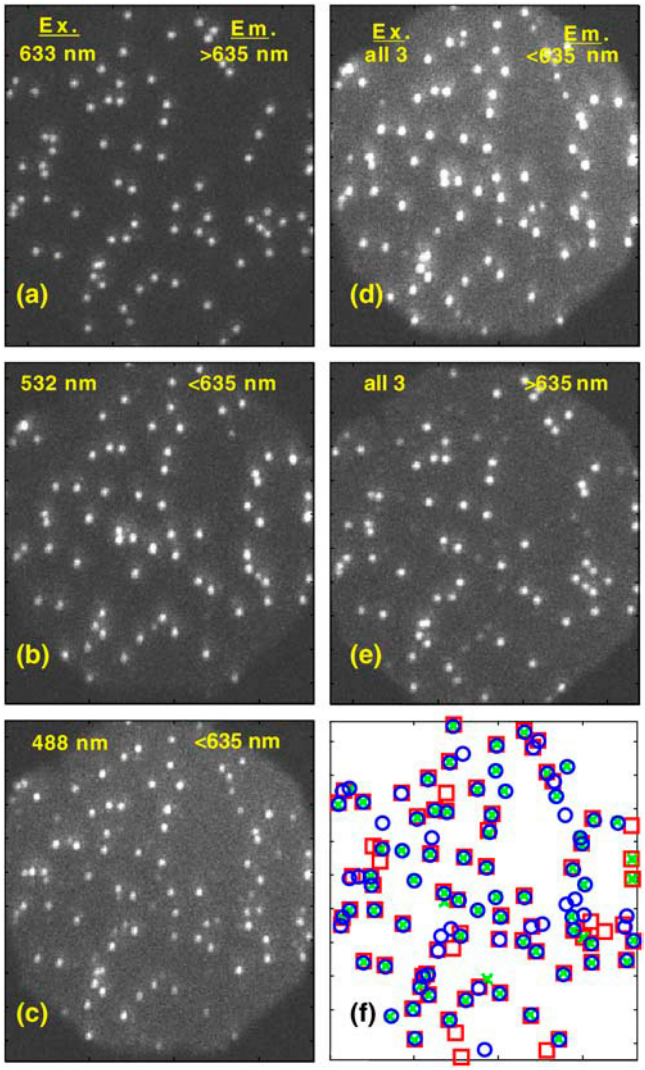

FIGURE 8 Field of DNA molecules hybridized to oligonucleotides labeled with three different dyes (see Fig. 4). (*a–e*) Fluorescence images (18.3 × 20.2 μm) of the same field excited with a single laser wavelength (Ex) of (*a*) 633, (*b*) 532, or (*c*) 488 nm (close to the excitation maxima of Cy5, Cy3, and Alexa 488, respectively), or (*d–e*) with all three lasers simultaneously. Emitted fluorescence (Em) images were collected from either the long- (>635 nm; *a* and *e*) or short- (<635 nm; *b–d*) wavelength area of the dual-view optics image. The duplex DNAs were preformed on a fused silica coverslip, and unbound dye-labeled oligonucleotides were flushed from the cell before imaging. Each image is an average of 20 0.1-s duration frames. Typical single-molecule spots consist of ~3000, ~3600, and ~2300 photons in *a–c*, respectively. (*f*) Overlaid positions of each kind of dye molecule as detected in (*a*) (Cy5; *red open boxes*), (*b*) (Cy3; *green* ×), and (*c*) (Alexa 488; *blue open circles*). Some DNA molecules do not contain all three dye moieties, due either to incomplete labeling or to photobleaching.

The ability to detect which of the three dyes is present at each point in the field in a given frame allows us to examine the sequence and kinetics of reaction steps by which dye-labeled molecules assemble into a complex. As an example, we studied the oligonucleotide hybridization

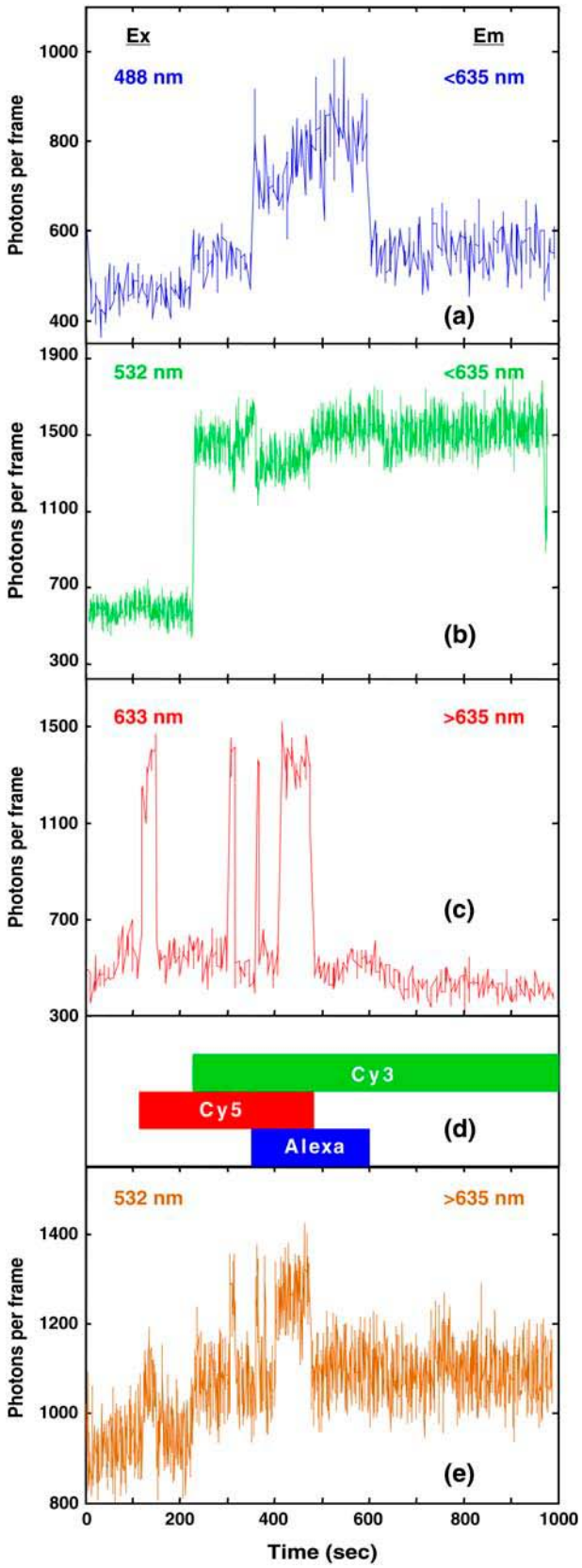

FIGURE 9 Binding of dye-labeled oligonucleotides to a single immobilized DNA molecule. The binding reaction was initiated by introducing a mixture of the three different dye-labeled oligonucleotides labeled with Alexa 488, Cy3, and Cy5 (6.3 nM, 5.0 nM, and 2.0 nM, respectively) into a glass flow chamber with the surface-immobilized target ssDNA. The oligonucleotides were present in solution throughout the duration of the recordings. Fluorescence from the dyes was detected by cyclically exciting the sample at 488 nm (five 200-ms frames), 532 nm (25 frames), and 633 nm (five frames). (*a–c*, *e*) Time records of integrated fluorescence from a single spot in the field (0.4 μm^2) recorded with the specified excitation and emission wavelengths. Zero emission is taken to be the signal recorded when the camera is shuttered. Presence of Alexa 488, Cy3, and Cy5 (*d*) were determined from records (*a–c*), respectively. Record (*e*) shows signals due to cross excitation of Cy5, FRET to Cy5, and leak-through of Cy3 emission into the >635-nm detection channel.

reaction used to form the triply labeled DNA (Figs. 4 and 8). A single surface-immobilized target DNA chosen for analysis first bound the Cy5-labeled oligonucleotide, then Cy3, then Alexa 488 (Fig. 9). The signals for binding and subsequent photobleaching (or detachment) of the three dyes are clearly resolved in the three detection channels (Fig. 9, *a–c*). The intensity fluctuations seen in Fig. 9 *c* are presumed to arise not from detachment and rebinding of the dye but rather from the blinking or optical switching previously reported to be characteristic of the Cy5 fluor (14,15).

In addition to displaying the abrupt increases and decreases from dye-labeled oligonucleotide binding and photobleaching, the fluorescence records also display smaller discontinuities. Two examples are 1), the step increase at 230 s in Fig. 9 *a*, which arises from the slight cross-excitation of Cy3 by the 488-nm laser; and 2), the transient decrease at 360–470 s in Fig. 9 *b*, which is likely due to weak FRET from Cy3 to Cy5, as suggested by the increase observed during the same time period in Fig. 9 *e*. Since each of these discontinuities is comparatively small and arises from a well-understood source, they do not impair interpretation of the records. It remains straightforward to discern the times and order of the oligonucleotide binding events.

The ability to observe binding reactions of different oligonucleotides to the same individual DNA molecule allows the rate constants of each binding reaction and the extent to which the different reactions are interdependent to be directly determined. For example, we can readily measure the aggregate rates for hybridization of each dye-labeled oligonucleotide (Fig. 10 *a*). For the hybridization of the Cy5-, Cy3-, and Alexa 488-labeled oligonucleotides, we measured aggregate second-order rate constants ($27.5 \pm 0.3 \times 10^5$, $2.21 \pm 0.01 \times 10^5$, and $0.564 \pm 0.004 \times 10^5$ M^{-1} s^{-1}, 0.95 confidence interval) that vary over a range of ~50-fold. The wide range of rates measured for these oligonucleotides of similar length suggests that some of the reactions are slowed by secondary structure in the probe and/or target DNA strand.

Even in this comparatively simple reaction system, one might predict that the different binding steps are not independent: secondary structure in the target strand might be at least partially disrupted by binding of one probe oligonucleotide, resulting in faster binding of the second and third probes to react with the same target molecule. Such an effect

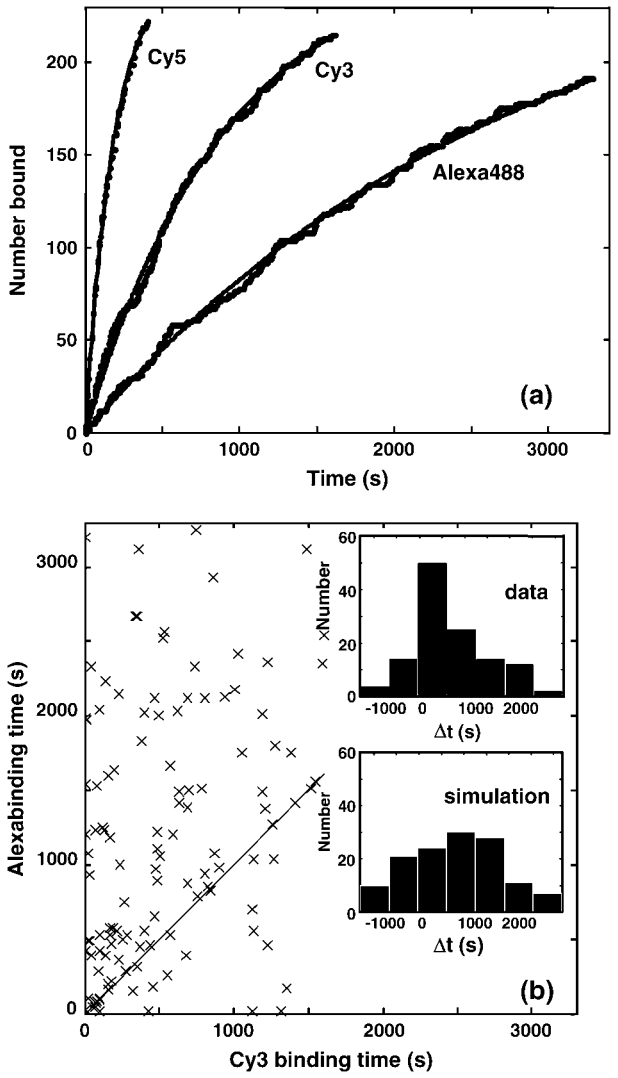

FIGURE 10 Time courses of dye-labeled oligonucleotide binding to multiple immobilized target DNA molecules in the same experiment shown in Fig. 9. These data were recorded from a single field of view containing ~260 target DNA molecules. (*a*) Cumulative number of observed binding events, n, for each oligonucleotide as a function of time, t, after the start of observation (*points*). One-parameter fits (*lines*) are to the function $n(t) = [n(t_{max})/(1 - \exp(-t_{max} / \tau))][1 - \exp(-t/\tau)]$, where t_{max} is the longest observation time for each oligonucleotide. The best-fit values of τ are 182, 905, and 2837 s, respectively, for the Cy5, Cy3, and Alexa 488 oligonucleotides. (*b*) Time until Cy3 oligonucleotide binding and time until Alexa 488 oligonucleotide binding for the 122 individual DNA molecules to which both oligonucleotides were observed to bind (observation times 1598 s for Cy3 and 3233 s for Alexa 488). Clustering of points near the line suggests that binding of the two oligonucleotides is not independent. (*Inset*) Histograms of Δt = (Alexa 488 oligonucleotide binding time) − (Cy3 oligonucleotide binding time) for the data (*top*) and for a simulation (*bottom*) based on the measured second-order rate constants and assuming independent binding of the two oligonucleotides. The large peak in the data histogram that is not seen in the simulation indicates an enhanced rate of Alexa 488 oligonucleotide binding to target DNAs on which the Cy3 oligonucleotide is already bound.

is apparent in a comparison of the time until binding of the Cy3 and Alexa 488 oligonucleotides to individual target DNA molecules (Fig. 10 *b*). These data reveal a tendency for Alexa 488-DNA to bind after Cy3-DNA that is more marked than would be expected for independent hybridization of the two oligonucleotides. Detailed analysis of the conditional binding probabilities (not shown) demonstrates that the rate constant for Alexa-488 binding is ~2-fold faster to complexes that have already bound Cy3-DNA.

DISCUSSION

This work presents a novel microscope design for multi-wavelength single-molecule total internal reflection fluorescence light microscopy. The data show that the instrument efficiently collects and detects emitted photons, giving total detected photon yields similar to those reported for other single-molecule fluorescence instruments. In addition, we demonstrate that the optical design directs the objective autofluorescence out of the imaging path, thus removing a significant contribution to background noise. Finally, we show by direct measurement that the optical design does not significantly broaden the microscope point spread function.

The total internal reflection fluorescence (TIRF) design presented here may have advantages over existing TIRF microscopy optical systems for certain types of experiments. The small broadband mirrors allow us to employ multiple excitation wavelengths without incurring the emission losses that would accompany use of the multi-wavelength dichroic mirror required in conventional epi-illuminated TIRF microscopes to separate the excitation and emission pathways. Both designs require wavelength-selective filters to remove scattered excitation light, but the notch filters used here have reflection bands that are less than half the width of the reflection bands for typical multi-wavelength dichroics.

Multi-wavelength excitation in single-molecule TIRF microscopy can also be achieved through a transillumination mode that uses a prism to couple the excitation beams through a coverslip on the side of the specimen distal to the objective (1,2,10). Like the design presented here, the prism approach also achieves low background by spatially segregating the excitation and emission pathways. However, through-objective TIRF optics reduce spherical aberration by imaging the surface of the coverslip closest to the objective, leave the other side of the sample free for use in combining single-molecule fluorescence with techniques such as laser trapping (16) or brightfield imaging (17), and may be simpler to maintain in alignment.

Multi-color fluorescence correlation spectroscopy represents an alternate approach that measures population distributions of complexes in solution (18,19). However, with the approach described here we demonstrate the ability to detect the binding of multiple molecules labeled with different dyes to an individual immobilized target. These are single-molecule kinetics experiments that allow direct measurement of all

relevant single-step binding (and dissociation) rate constants when experiments are performed with mixtures of probe molecules. This capability is demonstrated by the experiments in Figs. 9 and 10, in which hybridization of three differently labeled oligonucleotide probes to a single target DNA is observed. Such experiments can more easily reveal complex kinetic interdependencies (such as tendencies for one molecule to bind only after another has already bound) than conventional experiments that are restricted to observing the population-averaged properties of molecular ensembles.

Single molecule TIRF microscopy is generally applied with solution concentrations of the dye-labeled components at or below 50 nM to limit background fluorescence (20) (though specialized sample cells may extend this into the micromolar range (21)). There are numerous biological systems involving complexes that assemble with equilibrium dissociation constants $<10^{-8}$ M, and these are potential applications for the techniques described in this work. In this study, we chose a simple, artificial DNA hybridization reaction as an example that illustrates the capabilities of a multi-wavelength single-molecule fluorescence microscope to dissect the kinetic mechanism of a system undergoing multiple simultaneous binding reactions. However, we anticipate that a wide variety of other biologically interesting macromolecular systems can be analyzed in vitro using the same general approach. A simple extension of the experiments done here is to study the binding of dye-labeled proteins to a target DNA or RNA. Transient assembly of a specific complex of proteins on a nucleic acid scaffold to perform some particular function, followed by the dissociation of the complex once the function is completed, is a feature of such processes as DNA repair, replication, recombination, transcription, and RNA modification and splicing. In all such systems, the approach used here can follow the entire process of formation and breakdown of individual complexes, giving comprehensive information about the identities and numbers of each labeled protein that are associated with the nucleic acid at each point in time. Thus, such experiments can identify reaction pathways that are kinetically competent for the biological function and comprehensively characterize all relevant individual reaction steps.

SUPPLEMENTARY MATERIAL

An online supplement to this article can be found by visiting BJ Online at http://www.biophysj.org.

We thank Anne Gershenson and Doug Martin for comments on the manuscript.

This work was supported by grants from the National Institute of General Medical Sciences.

REFERENCES

1. Funatsu, T., Y. Harada, M. Tokunaga, K. Saito, and T. Yanagida. 1995. Imaging of single fluorescent molecules and individual ATP turnovers by single myosin molecules in aqueous solution. *Nature.* 374:555–559.
2. Margeat, E., A. N. Kapanidis, P. Tinnefeld, Y. Wang, J. Mukhopadhyay, R. H. Ebright, and S. Weiss. 2006. Direct observation of abortive initiation and promoter escape within single immobilized transcription complexes. *Biophys. J.* 90:1419–1431.
3. Rasnik, I., S. Myong, W. Cheng, T. M. Lohman, and T. Ha. 2004. DNA-binding orientation and domain conformation of the E. coli rep helicase monomer bound to a partial duplex junction: single-molecule studies of fluorescently labeled enzymes. *J. Mol. Biol.* 336: 395–408.
4. Blanchard, S. C., R. L. Gonzalez, H. D. Kim, S. Chu, and J. D. Puglisi. 2004. tRNA selection and kinetic proofreading in translation. *Nat. Struct. Mol. Biol.* 11:1008–1014.
5. Zhuang, X., L. E. Bartley, H. P. Babcock, R. Russell, T. Ha, D. Herschlag, and S. Chu. 2000. A single-molecule study of RNA catalysis and folding. *Science.* 288:2048–2051.
6. Deniz, A. A., T. A. Laurence, G. S. Beligere, M. Dahan, A. B. Martin, D. S. Chemla, P. E. Dawson, P. G. Schultz, and S. Weiss. 2000. Single-molecule protein folding: diffusion fluorescence resonance energy transfer studies of the denaturation of chymotrypsin inhibitor 2. *Proc. Natl. Acad. Sci. USA.* 97:5179–5184.
7. Hohng, S., C. Joo, and T. Ha. 2004. Single-molecule three-color FRET. *Biophys. J.* 87:1328–1337.
8. Pierce, D. W., and R. D. Vale. 1998. Assaying processive movement of kinesin by fluorescence microscopy. *Methods Enzymol.* 298:154–171.
9. http://www.brandeis.edu/projects/gelleslab/glimpse/glimpse.html
10. Axelrod, D. 1989. Total internal reflection fluorescence microscopy. *Methods Cell Biol.* 30:245–270.
11. Tokunaga, M., K. Kitamura, K. Saito, A. H. Iwane, and T. Yanagida. 1997. Single molecule imaging of fluorophores and enzymatic reactions achieved by objective-type total internal reflection fluorescence microscopy. *Biochem. Biophys. Res. Commun.* 235:47–53.
12. Kinosita, K. Jr., H. Itoh, S. Ishiwata, K. Hirano, T. Nishizaka, and T. Hayakawa. 1991. Dual-view microscopy with a single camera: real-time imaging of molecular orientations and calcium. *J. Cell Biol.* 115: 67–73.
13. Yildiz, A., J. N. Forkey, S. A. McKinney, T. Ha, Y. E. Goldman, and P. R. Selvin. 2003. Myosin V walks hand-over-hand: single fluorophore imaging with 1.5-nm localization. *Science.* 300:2061–2065.
14. Heilemann, M., E. Margeat, R. Kasper, M. Sauer, and P. Tinnefeld. 2005. Carbocyanine dyes as efficient reversible single-molecule optical switch. *J. Am. Chem. Soc.* 127:3801–3806.
15. Bates, M., T. R. Blosser, and X. Zhunag. 2005. Short-range spectroscopic ruler based on a single-molecule optical switch. *Phys. Rev. Lett.* 94:108101.
16. Lang, M. J., P. M. Fordyce, A. M. Engh, K. C. Neuman, and S. M. Block. 2004. Simultaneous, coincident optical trapping and single-molecule fluorescence. *Nat. Methods.* 1:133–139.
17. Nishizaka, T., K. Oiwa, H. Noji, S. Kimura, E. Muneyuki, M. Yoshida, and K. Kinosita Jr. 2004. Chemomechanical coupling in F1-ATPase revealed by simultaneous observation of nucleotide kinetics and rotation. *Nat. Struct. Mol. Biol.* 11:142–148.
18. Heinze, K. G., M. Jahnz, and P. Schwille. 2004. Triple-color coincidence analysis: one step further in following higher order molecular complex formation. *Biophys. J.* 86:506–516.
19. Burkhardt, M., K. G. Heinze, and P. Schwille. 2005. Four-color fluorescence correlation spectroscopy realized in a grating-based detection platform. *Opt. Lett.* 30:2266–2268.
20. Ishijima, A., H. Kojima, T. Funatsu, M. Tokunaga, H. Higuchi, H. Tanaka, and T. Yanagida. 1998. Simultaneous observation of individual ATPase and mechanical events by a single myosin molecule during interaction with actin. *Cell.* 92:161–171.
21. Levene, M. J., J. Korlach, S. W. Turner, M. Foquet, H. G. Craighead, and W. W. Webb. 2003. Zero-mode waveguides for single-molecule analysis at high concentrations. *Science.* 299:682–686.